Advanced Composites and Hybrid Materials (2024) 7:6
https://doi.org/10.1007/s42114-023-00821-2

RESEARCH

Intelligent hydrogel on–off controller sensor for irrigation

Xue-Qing Zhan[1] · Zhuo-Qing Ran[1] · Hong-Yu Bao[1] · Qin Ye[1] · Han Chen[1] · Qiang Fu[2] · Wang Ni[1] · Jia-Min Xu[1] · Ning Ma[1,3] · Fang-Chang Tsai[1]

Received: 29 March 2023 / Revised: 8 December 2023 / Accepted: 22 December 2023 / Published online: 31 December 2023

Abstract
As a functional material, hydrogels hold promise in agricultural irrigation, potentially solving the problem of low utilization of irrigation water from the source. To enable more intuitive monitoring of soil moisture and achieve on-demand irrigation, a conductive hydrogel is being explored as a solenoid valve controller for intelligent irrigation. Here, intelligent hydrogel poly (acrylic acid-co–N-methylolacrylamide)/poly(3,4-ethylenedioxythiophene):polystyrene sulfonate, P(AA-co–N-MA)/PEDOT:PSS, with a dual network was synthesized under mild conditions through Na_2SO_3-APS (ammonium persulfate) initiation system. The structural design endows the hydrogel with excellent mechanical properties (elongation at break up to 2400%) and sensitive sensing performance (gauge factor, GF, is 8.14). The anti-fatigue properties of the hydrogel have proved that the material has good durability and good service life as a sensing material. In addition, by incorporating the relationship between moisture and conductivity, the hydrogel could be utilized as a controller for irrigation valves, enabling intelligent irrigation and effective conservation of water resources through soil moisture monitoring.

Keywords Hydrogel · Dual network · Durability · Intelligent irrigation · Solenoid valve controller

1 Introduction

Limited freshwater resources are now seriously threatened by environmental degradation, climate change, and over-exploitation. According to the Food and Agriculture Organization of the United Nations, freshwater per capita has decreased by 20% over the previous two decades, with approximately 60% of irrigated farmland experiencing water scarcity. Furthermore, more than 70% of global freshwater flow is allocated for agricultural purposes [1]. To address this issue, various technologies are being explored to enhance agricultural water efficiency, aiming to reduce the demand for freshwater resources worldwide. The technologies being researched at the moment to increase the effectiveness of agricultural water use primarily include the following: (i) Soil amendment: Hydrogel is a soil additive that can be used to irrigate plants even in arid or desert environments by holding irrigation water or rainwater when placed into the soil [2–4]. (ii) Wastewater irrigation: The heavy metal ions in the wastewater are filtered, which makes it possible to use the effluent for irrigation [5–15]. (iii) Collection of atmospheric water: To actively capture water vapor from the environment and gather fresh water, hygroscopic materials can be used [16–19]. (iv) Intelligent irrigation: Automatic control technology is adopted to implement water-saving irrigation [20–22]. The advantages of science, technology, intelligence, and efficiency make the intelligent irrigation system superior to the traditional one. It can prevent overwatering and lower operational costs by limiting water use at the source and increasing the rate at which water resources are utilized [23–25].

✉ Ning Ma
ningma@hubu.edu.cn

✉ Fang-Chang Tsai
tfc0323@gmail.com

[1] Hubei Key Laboratory of Polymer Materials, Key Laboratory for the Green Preparation and Application of Functional Materials (Ministry of Education), Hubei Collaborative Innovation Center for Advanced Organic Chemical Materials, School of Materials Science and Engineering, Hubei University, Wuhan 430062, China

[2] Department Beijing National Laboratory for Molecular Sciences, College of Chemistry and Molecular Engineering, Peking University, Beijing 100871, China

[3] State Key Laboratory of Biocatalysis and Enzyme Engineering, School of Life Sciences, Hubei University, Wuhan 430062, China

Although agricultural activities rely on many factors of the soil–water-plant-atmosphere system, adequate irrigation management can be established based on monitoring soil moisture [26]. On this basis, soil moisture sensors have been widely studied [27]. As a crosslinked three-dimensional hydrophilic polymer [28–31], hydrogels are a special moisture-sensitive material that can be incorporated into mechanical systems to control irrigation according to gel swelling [32–34]. However, as a kind of intelligent material, conductive hydrogels offer additional advantages in their ability to function as sensors, detecting external stimuli and converting them into electrical signals [35–41]. Polyacrylic acid is a water-soluble polymer with good biocompatibility and hydrophilicity, which is the best choice for a conductive hydrogel substrate. However, in the existing studies, the synthesis conditions of polyacrylic gel–based products are more stringent—high synthesis temperature, long reaction time, inert gas environment, etc. [42–45], which is not conducive to industrial conversion. Therefore, it is necessary to improve the synthesis process of polyacrylic-based gels.

Here, soluble polymer polyacrylic acid was selected as the substrate, doped with the conductive polymer poly(3,4-ethylenedioxythiophene)–polystyrene sulfonate (PEDOT:PSS) with good conductivity and the Na_2SO_3 (sodium sulfite)–APS (ammonium persulfate) oxidation–reduction initiation system was used for the reaction to synthesize the polyacrylic-based conductive hydrogel P(AA-co–N-MA)/PEDOT:PSS under mild conditions. Firstly, N-methylolacrylamide (N-MA) was used to form a crosslinked network with polyacrylic acid (PAA). Then, PEDOT:PSS was doped into the crosslinked network to form a dual network structure to improve mechanical properties. Due to the dual network design, the mechanical properties of the polyacrylic-based hydrogel are significantly improved—a tensile strain of up to 2400% was achieved. Meanwhile, the doping of PEDOT:PSS improves its conductivity—from 0.18 to 0.26 s/m. Moreover, as a conductive hydrogel, P(AA-co–N-MA)/PEDOT:PSS hydrogel enables to sense mechanical reactions with good sensitivity, and its GF reaches 8.14. In addition, the variation of water content and conductivity of P(AA-co–N-MA)/PEDOT:PSS hydrogel at different temperatures (0 ℃, 25 ℃, 45 ℃, 70 ℃) makes it a potential soil moisture sensor. The toughness and conductivity of the hydrogel remain in such a wide temperature range, indicating its high environmental applicability and suitability for use in various climates. Here, we consider it as a controller for an intelligent irrigation system to utilize water resources by irrigating on demand.

2 Synthesis

2.1 Materials

All chemicals and reagents used were of analytical grade. N-methylolacrylamide (N-MA) and poly(3,4-ethylenedioxythiophene)–polystyrene sulfonate (PEDOT:PSS) were purchased from Aladdin. Acrylic acid (AA), anhydrous sodium sulfite (Na_2SO_3), and ammonium persulfate (APS) were purchased from Sinopharm Chemical Reagent Co., Ltd.

Synthesis of PAA hydrogel PAA hydrogel was prepared as the following experiment. Six milliliters of AA, 25 mg (0.11 mmol) APS, and 9.2 mg (0.073 mmol) Na_2SO_3 were transferred to a 100-mL flask containing 20 mL of water. The mixture was stirred at room temperature (RT) for 5 min at a rotation speed of 300 r/min, then reacted for 30 min at 60 ℃ without stirring.

Synthesis of PAA/PEDOT: PSS hydrogel PAA/PEDOT:PSS hydrogel was prepared as the following experiment. Six milliliters of AA, 0.4 mL of PEDOT:PSS, 25 mg (0.11 mmol) APS, and 9.2 mg (0.073 mmol) Na_2SO_3 were transferred to a 100-mL flask containing 20 mL of water. The mixture was stirred at RT for 5 min at a rotation speed of 300 r/min, then reacted for 10 min at 45 ℃ without stirring.

Synthesis of P(AA-co–N-MA)/PEDOT: PSS hydrogel P(AA-co–N-MA)/PEDOT:PSS hydrogel was prepared as the following experiment. Six milliliters of AA, 0.4 mL of PEDOT:PSS, 600 mg (5.93 mmol) N-MA, 25 mg (0.11 mmol) APS, and 9.2 mg (0.073 mmol) Na_2SO_3 were transferred to a 100-mL flask containing 20 mL of water. The mixture was stirred at RT for 5 min at a rotation speed of 300 r/min, then reacted for 10 min at 45 ℃ without stirring.

2.2 Characterization

Scanning electron microscopy (SEM) was carried out by Zeiss Sigma 500 field emission SEM. ATR-FTIR analysis was recorded by Thermo Fisher (Nicolet iS50) with the ATR diamond crystal. In situ temperature-variable FTIR measurement was recorded on the Bruker (Tensor 27) FTIR spectrometer, heating from 20 to 80 ℃, at every 5 ℃ by transmission mode. The hydrophilicity of the hydrogel is characterized by a contact angle (CA) measuring instrument (Power each JC2000D1). Thermogravimetric analysis (TGA) measurement is performed on the 1 Star^e by scanning the temperature range from 30 to 800 ℃ (10 ℃ min^{-1}) under airflow. Differential scanning calorimetry (DSC) measurement is performed on the TA Q2000 scanning from 40 to 140 ℃ at a scanning rate of 5 ℃ min^{-1} under N_2 flow.

Water stability measurements Hydrogel blocks of similar size were placed in an oven at 45 ℃ for 48 h, and the weight was recorded as W_0. The dried hydrogel block was then submerged in deionized water at room temperature for 48 h,

removed, and placed back in a 45 ℃ oven for 48 h. It was then weighed as W_1, and the weight loss rate was calculated as Eq. 1. Three sets of parallel experiments were set up and the mean values were taken.

$$\text{Weight loss}\,(\%) = (1 - W_1/W_0) * 100\% \quad (1)$$

Rheological measurements The hydrogels were conducted on TA Discovery HR-1 Hybrid Rheometer with parallel plate geometry (25-mm diameter) over a temperature range of 30 to 140 ℃ at $\omega = 10$ rad s^{-1} and $\gamma = 0.1\%$. Frequency sweep measurements were measured at $\gamma = 0.1\%$ mode over a frequency range of 0.1–100 Hz (0.628–628 rad s^{-1}) at 30 ℃. Amplitude sweep measurements were performed at $\omega = 10$ rad s^{-1} mode over a strain range of 0.1–100% at 30 ℃.

Tensile measurements Tensile measurement was carried out on a universal tensile high and low temperature (Instron 68TM-10) with a 1 kN transducer at a 50 mm/min tensile rate. The hydrogels were cut into a long strip (test size $50 \times 10 \times 3$ mm^3) for testing. Through the same specimen at a speed of 20 mm/min, the cyclic tensile and compressive loading and unloading test was carried out to study the self-healing performance.

Electrochemical measurement The conductivity tests were carried out using an electrochemical workstation (CHI 660e) at frequencies ranging from 1 to 10^5 Hz with an amplitude of 10 mV. The conductivity σ is obtained from the Nyquist diagram using Eq. 2,

$$\boldsymbol{\sigma} = \mathbf{d}/(\mathbf{R} * \mathbf{S}) \quad (2)$$

where d is the thickness of the sample (the distance between adjacent electrodes), R is the bulk resistance, and S is the contact area between the sample and the electrode.

3 Results and discussion

The one-pot preparation process of the conductive hydrogel was composed of a P(AA-co–N-MA) network doped with PEDOT:PSS (Fig. 1a). The P(AA-co–N-MA) network mainly comprises two linear polymerization networks, PAA self-polymerization and PAA and N-MA crosslinking networks, which are formed by heating and then polymerization in an aqueous solution. PEDOT:PSS is uniformly distributed into the P(AA-co–N-MA) network during polymerization. Generally, the polymerization conditions of PAA-based gel are harsh, and not conducive to industrial conversion. Therefore, to promote the industrialization process of PAA-based gel, Na_2SO_3-APS redox initiator system is used to make the reaction conditions mild and enable rapid polymerization at lower temperatures (45 ℃ for 10 min). The redox initiator system mainly uses the free radical generated by the electron transfer between the oxidant and reducing agent to initiate the polymerization reaction, leading to improving reaction rates and reducing energy consumption [46]. The comparison of the synthesis process of PAA-based hydrogel between this work and the previous one is shown in Table S1, indicating that this work has more advantages. The interaction forces of P(AA-co–N-MA)/PEDOT:PSS hydrogel contain hydrogen bonds and electrostatic interactions, as shown in Fig. 1a. As a result, a network hydrogel with high elasticity is produced (Movie S1). The transmittance of P(AA-co–N-MA)/PEDOT:PSS hydrogel in the visible light range reaches about 80% (Fig. S1).

To prove the internal structure and interaction of the hydrogel, SEM and FTIR were carried out. As shown in Fig. 1b–d, the difference in the microscopic morphology of the hydrogels is clearly found. PAA hydrogel is in the shape of polymer chain segments, PAA/PEDOT:PSS is a lamellar network, and P(AA-co–N-MA)/PEDOT:PSS is a prominent network structure. To verify the internal interaction of hydrogel, ATR-FTIR of PAA, PAA/PEDOT:PSS, and P(AA-co–N-MA)/PEDOT:PSS hydrogels is present in Fig. 1e. The FTIR spectrum of PAA exhibits $\nu(COO^-)$ bands at 1548 cm^{-1} and 1412 cm^{-1}, $\nu(CH_2)$ bands at 2854 cm^{-1} and 2926 cm^{-1}, and the peak at 1710 cm^{-1} and 3215 cm^{-1} corresponds to $\nu(C=O)$ and OH of a dimer, respectively [44]. With the addition of PEDOT:PSS and N-MA, the peak of OH of dimer becomes weaker. After the addition of N-MA, the FTIR spectrum of P(AA-co–N-MA)/PEDOT:PSS appears to peak at 1105 cm^{-1} and 1173 cm^{-1} for ν(C–O–C), and the peak at 1656 cm^{-1} corresponds to ν(N–H). Combining these results indicates that AA and N-MA are chemically crosslinked. Furthermore, with PEDOT:PSS and N-MA, the hydrogel changes from hydrophilic to hydrophobic, as presented in Fig. 1f. During the synthesis of P(AA-co–N-MA)/PEDOT:PSS hydrogel, esterification of N-MA and PAA occurred, leading to a reduction in the number of hydrophilic groups -COOH, thereby weakening the hydrophilicity of the hydrogel. And the phenomenon is also corresponding to IR results. By employing peak-splitting treatment on the characteristic C=O peaks, distinct peaks for carboxylic acid and dimeric carboxylic acid were obtained, as shown in Fig. S2. According to the curve-fitting parameters (Table S2), the C=O peak area of carboxylic acid/C=O peak area of dimeric carboxylic acid decreased with the modification. This decrease in peak area suggests a reduction in the number of -COOH groups of the hydrogel, indicating an increase in hydrophobicity. Overall, the PAA self-polymerization linear network and the linear network formed by chemical crosslinking of AA and N-MA form the polymer network of P(AA-co–N-MA). The intermolecular interaction between P(AA-co–N-MA) and PEDOT:PSS

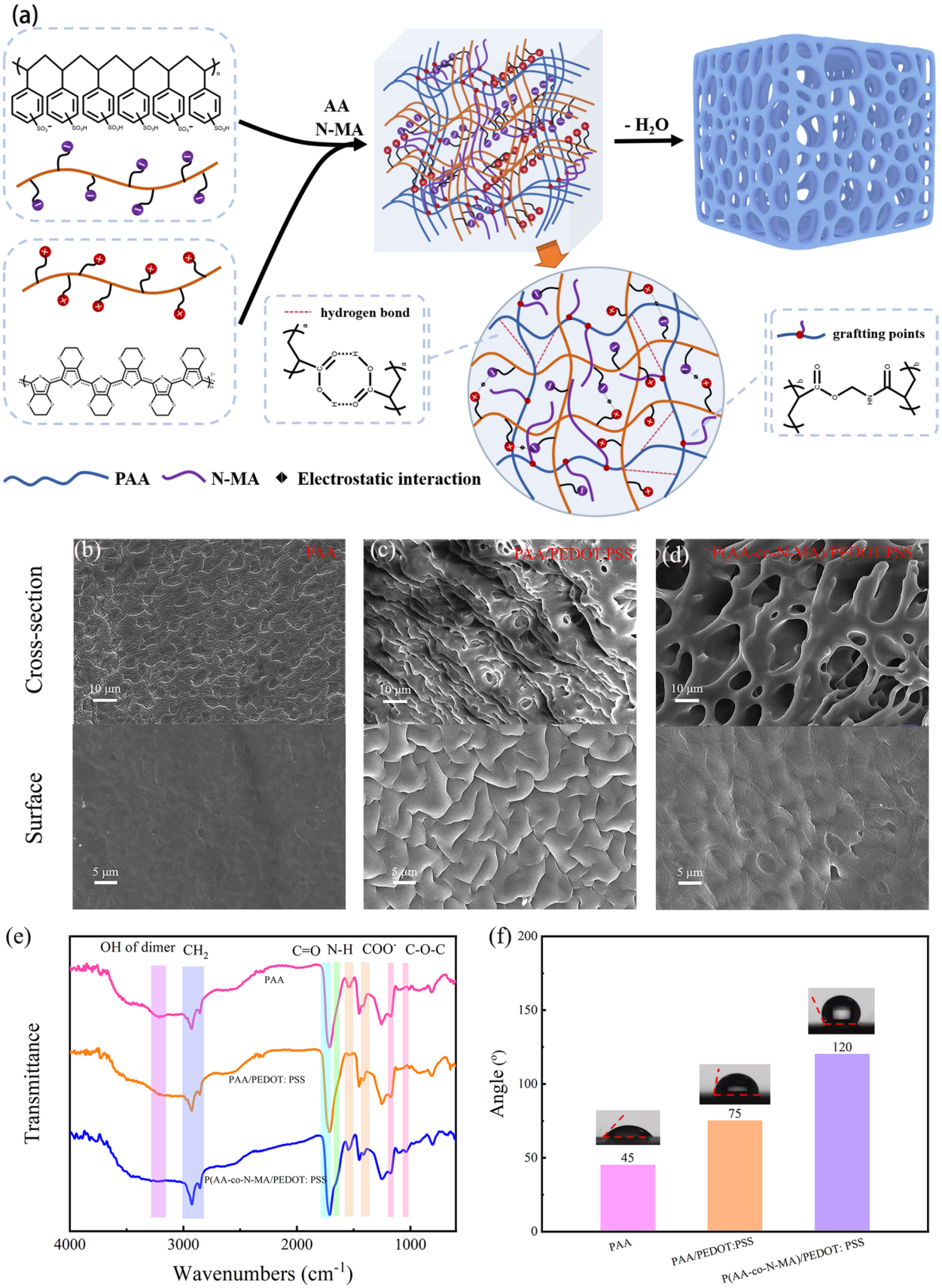
(a)
AA
N-MA
- H2O
hydrogen bond
graftting points
PAA
N-MA
Electrostatic interaction
(b)
PAA
(c)
PAA/PEDOT:PSS
(d)
P(AA-co-N-MA)/PEDOT:PSS
Cross-section
Surface
10 μm
5 μm
(e)
OH of dimer
CH2
C=O
N-H
COO-
C-O-C
PAA
PAA/PEDOT: PSS
P(AA-co-N-MA/PEDOT: PSS
Transmittance
Wavenumbers (cm-1)
4000
3000
2000
1000
(f)
Angle (°)
45
75
120
PAA
PAA/PEDOT:PSS
P(AA-co-N-MA)/PEDOT: PSS

◂**Fig. 1** **a** Schematic illustration of preparation P(AA-co–N-MA)/PEDOT: PSS hydrogel. Cross-section and surface morphology SEM images of **b** PAA, **c** PAA/PEDOT: PSS, and **d** P(AA-co–N-MA)/PEDOT: PSS hydrogels. **e** FTIR spectra of the PAA, PAA/PEDOT: PSS, and P(AA-co–N-MA)/PEDOT: PSS hydrogels. **f** Contact angles of PAA, PAA/PEDOT: PSS, and P(AA-co–N-MA)/PEDOT: PSS hydrogels

includes the dual network design structure, and the design enhances the mechanical properties of the hydrogel [47].

Excellent mechanical properties are indispensable for ensuring the durability and stability of flexible sensing material. The excellent mechanical properties are because the chemical bonds of crosslinked network are more substantial than the hydrogen bonds before modification, as seen from the schematic diagram (Fig. 2a). Figure 2b illustrates that P(AA-co–N-MA)/PEDOT:PSS hydrogel has high ductility and is easily stretched to 2400% without breaking. And the result is echoed with thermal analysis, as shown in Fig S3. The changes in DSC data during the modification of hydrogel also explain why the reaction conditions become mild during the modification process. With the addition of PEDOT:PSS, the Tm of hydrogel decreased from 103 to 80 ℃, and the introduction of N-MA increased the Tm of P(AA-co–N-MA)/PEDOT:PSS hydrogel to 87 ℃ and appeared crosslinked peak. At the same time, all the peaks of P(AA-co–N-MA)/PEDOT:PSS hydrogel disappeared after the second test, and the change of the final decomposition temperature of TGA demonstrates the chemically crosslinked effect of the hydrogel. With the addition of N-MA, the final decomposition temperature of hydrogel increased, and the higher the amount, the higher the temperature. The water stability test further illustrates the chemical crosslinking of the hydrogel, and the weight loss of hydrogels is calculated according to Eq. 1. After being soaked in water for 48 h, only P(AA-co–N-MA)/PEDOT:PSS hydrogel shows tiny changes (Fig. S4). Overall, chemically crosslinked provides the possibility of dual network design and improves the mechanical properties of the hydrogel. The difference in mechanical properties between hydrogels also illustrates the importance of dual network structure.

Typical stress–strain curves and mechanical properties of hydrogels at different temperatures are shown in Fig. S5. It is worth mentioning that hydrogel, after N-MA treatment, dramatically improves mechanical strength and elongation. P(AA-co–N-MA)/PEDOT:PSS hydrogel exhibited superior tensile strain relative to PAA and PAA/PEDOT:PSS hydrogels. At 25 ℃, the P(AA-co–N-MA)/PEDOT:PSS hydrogel has a tensile fracture strength of 137 kPa when the strain is 2400%. Under the same conditions, the strain of P(AA-co–N-MA)/PEDOT:PSS hydrogel is 3–4 times that of PAA and PAA/PEDOT:PSS hydrogels and the tensile fracture strength is two times than that. As the temperature increases, although the tensile strain of P(AA-co–N-MA)/PEDOT:PSS hydrogel is reduced, the tensile fracture strength of the hydrogel has been enhanced (Fig. 2c). Compared with PAA and PAA/PEDOT:PSS hydrogels, its tensile strain is still advantageous—it maintains almost 60% of the tensile strain at room temperature. Based on the structural analysis and thermodynamic analysis of the hydrogel, the introduction of N-MA forms the P (AA-co–N-MA) crosslinking network and forms a dual network with PEDOT:PSS, which improves the mechanical properties of the hydrogel. These indicated that the introduction of N-MA plays a vital role in the excellent mechanical properties of P(AA-co–N-MA)/PEDOT:PSS hydrogel. It also further proves that dual network structure has obvious advantages in improving the mechanical properties of materials.

The anti-fatigue performance of hydrogel determines its service life as a sensor. The hydrogel was subjected to continuous loading–unloading cycles to study the anti-fatigue behavior. As shown in Fig. 3a, cyclic tensile tests of P(AA-co–N-MA)/PEDOT:PSS hydrogel under different strains showed that the hysteresis loops increased correspondingly with increasing strains. According to the calculation results of dissipated energy, the hysteresis energy increases linearly from 1.6 to 17.2 MJ/m^3 as the strain increases from 100 to 600% (Fig. 3b). The anti-fatigue behavior of P(AA-co–N-MA)/PEDOT:PSS hydrogel was carried out by cyclic loading–unloading experiments, as presented in Fig. 3c, d. After the first cycle, the hysteresis loop becomes narrower until a steady state is reached. The hysteresis energy achieves a relatively stable value of 2.8 MJ/m^3 after the 10th loading–unloading cycle. These results indicated that the anti-fatigue performance of the hydrogel is good. Research on the energy dissipation mechanism of P(AA-co–N-MA)/PEDOT:PSS hydrogel was studied through the cyclic tensile test. Due to the electrostatic and hydrogen bond interactions in the P(AA-co–N-MA)/PEDOT:PSS hydrogel, the hydrogel effectively dissipates energy during stretching and compression [48]. In addition, P(AA-co–N-MA)/PEDOT:PSS hydrogel was subjected to cyclic compression testing at 82% maximum strain, as shown in Fig. 3e, f. It was observed that after the 10th cycle, the cyclic loading–unloading curves almost overlap, and the hysteresis energy stabilizes at 4 MJ/m^3. This further proves that the P(AA-co–N-MA)/PEDOT:PSS hydrogel possesses excellent anti-fatigue performance.

The rheological property is an essential indicator to assess the viscoelasticity of the hydrogel. As depicted in Fig. S6a–c, the modulus of the hydrogels started to decrease at certain temperatures. The corresponding temperatures at which the modulus began to decline of PAA, PAA/PEDOT:PSS, and P(AA-co–N-MA)/PEDOT:PSS hydrogels were 102 ℃, 83 ℃, and 98 ℃, respectively. This trend is consistent with the variation of T_m obtained from DSC.

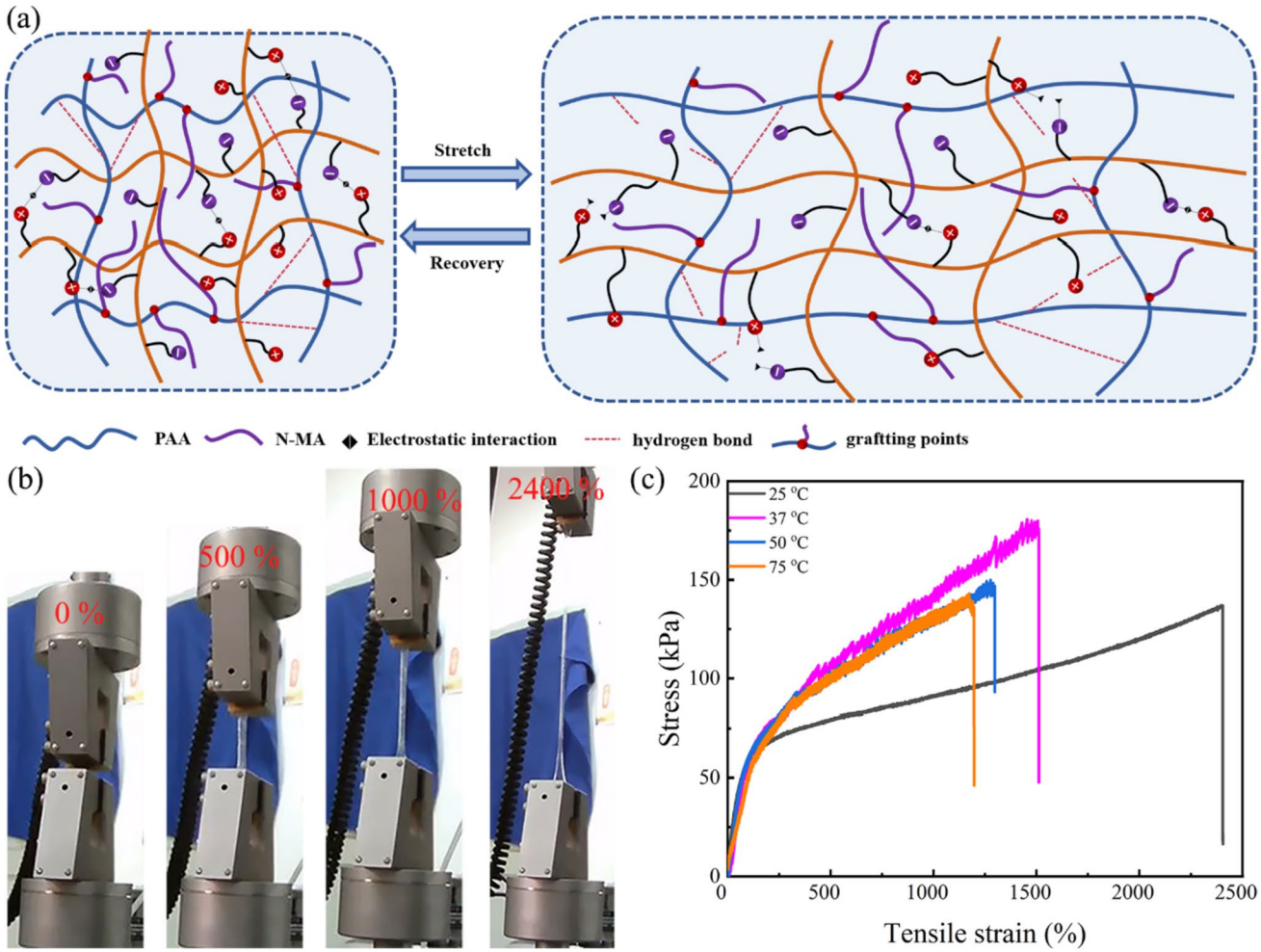

Fig. 2 Mechanical properties of hydrogels. **a** Schematic illustration of the enhancement of the mechanical properties of P(AA-co–N-MA)/PEDOT: PSS hydrogel. **b** Photographs that record the stretching process of the hydrogel. **c** Tensile curves of P(AA-co–N-MA)/PEDOT: PSS hydrogel at different temperatures

In particular, the storage modulus (G′) of P(AA-co–N-MA)/PEDOT:PSS hydrogel exhibited a distinctive behavior, initially increasing and decreasing after 98 ℃. The increase of G′ before 98 ℃ was attributed to the enhancement of molecular chain entanglement, resulting from reduced water content and weakened hydrogen bonding forces as the temperature rises. However, the subsequent decrease of G′ was due to the destruction of the interaction within the hydrogel network at higher temperatures. As shown in Fig. S6e–f, with the increase of frequency and strain, the G′ of P(AA-co–N-MA)/PEDOT:PSS hydrogel consistently remained higher than the G″ (loss modulus), showing its predominantly elastic properties.

Due to the dual network design, the hydrogel retains part of its self-healing ability. In situ temperature-variable FTIR spectra of P(AA-co–N-MA)/PEDOT:PSS hydrogel at 20–80 ℃ were recorded to certify the thermal stability of the interaction. As the temperature rises, the loss of H_2O weakens the hydrogen bond (Fig. S7). The shift of ν(C = O) and OH of the dimer corresponds to the weakening of the hydrogen bond, as presented in Fig. 4a, b, respectively [49]. At the same time, the peak intensity of ν(N–H) is weakened, indicating that the dipole moment is reduced and the polarity is weakened. The results show that the water content affects the strength of the hydrogen bond of the hydrogel, and thus affects the self-healing ability of the hydrogel. The diagram illustrates the internal interaction of P(AA-co–N-MA)/PEDOT:PSS hydrogel and explains the mechanism of the self-healing of the hydrogel (Fig. 4c). The schematic diagram shows that the reversible self-healing behavior mainly depends on physical interactions, such as hydrogen bonding and electrostatic interaction. As shown in Fig. 4d, bring the two pieces of P(AA-co–N-MA)/PEDOT:PSS hydrogel together at the humidity of RH 100%. After 12 h, the boundary of the sample connection became lighter. It could not break when stretched, indicating that P(AA-co–N-MA)/

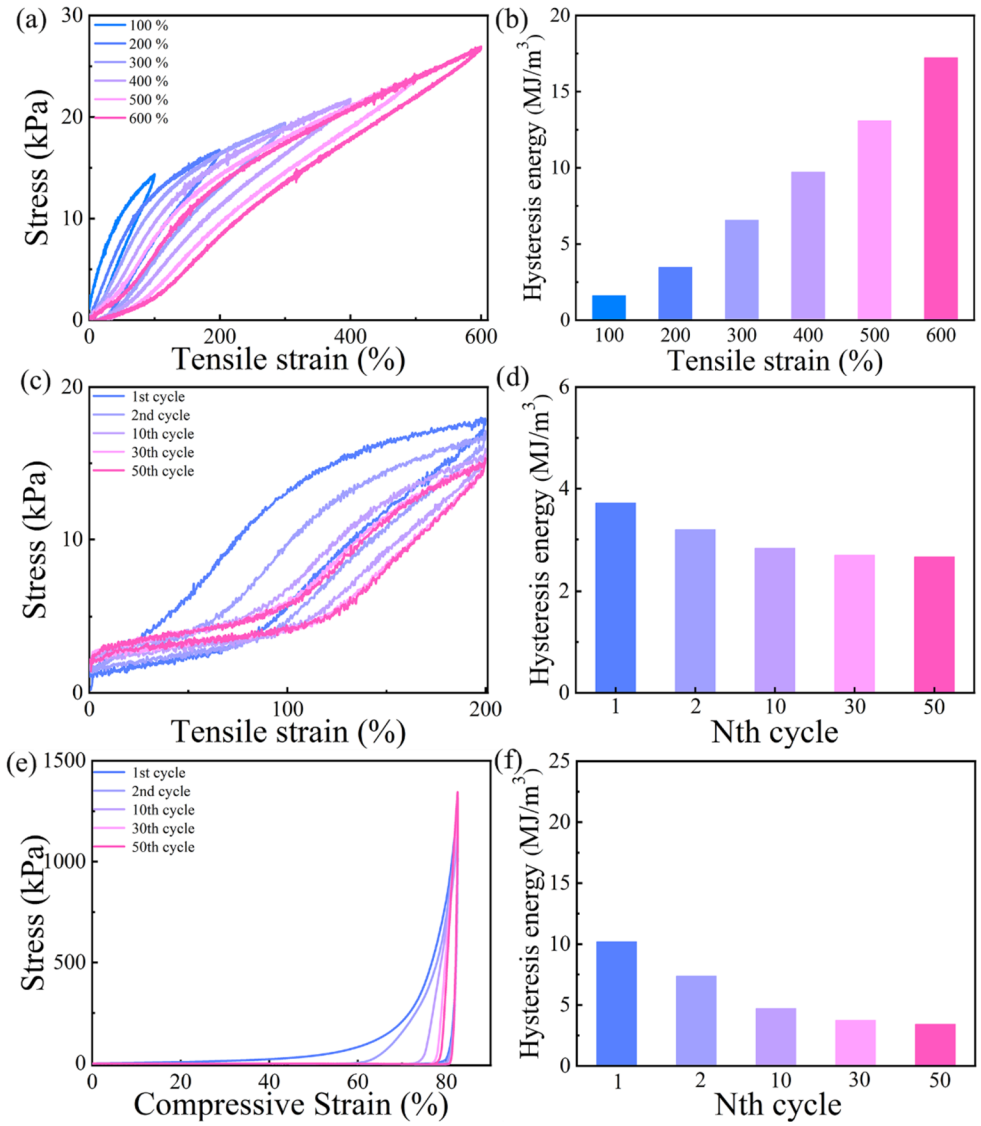

Fig. 3 Anti-fatigue properties of the hydrogel. **a** Continuous cyclic stress–strain curve of P(AA-co–N-MA)/PEDOT: PSS hydrogel with gradually increasing strain and **b** the corresponding hysteresis energy. **c** Cyclic tensile curves of 50 consecutive cycles of P(AA-co–N-MA)/PEDOT: PSS hydrogel at a fixed maximum strain of 200% and **d** the corresponding hysteresis energy. **e** Cyclic compression curves of 50 consecutive cycles of P(AA-co–N-MA)/PEDOT: PSS hydrogel at a fixed maximum strain of 82% and **f** the corresponding hysteresis energy

PEDOT:PSS hydrogel has self-healing properties. Subsequently, the hydrogel was 650% fixed and stretched continuously for several self-healing cycles. The possible reason for the tensile stress becoming more robust after the first day is the loss of moisture in the sample over time (Fig. 4e). In addition, P(AA-co–N-MA)/PEDOT:PSS hydrogel acts as a conductor in the circuit (Fig. 4f). Its fracture and connection affect the path of the circuit, showing rapid electrical self-healing ability. According to Fig. 4g, after the hydrogel is in contact, the direct current of the self-healing P(AA-co–N-MA)/PEDOT:PSS hydrogel recovers to a horizontal transient fluctuation within 0.9 s.

As a mechanically responsive flexible material, the hydrogel enables to act as a sensor to sense external stimuli and convert them into electrical signals. Based on this application, the conductivity of the material is essential. The conductivity is calculated according to Eq. 2, and the excellent conductivity of P(AA-co–N-MA)/PEDOT:PSS hydrogel is shown in Figs. 5a and S8. As shown in Fig. 5b, c and Movie S2, the illuminance varies nonlinearly with

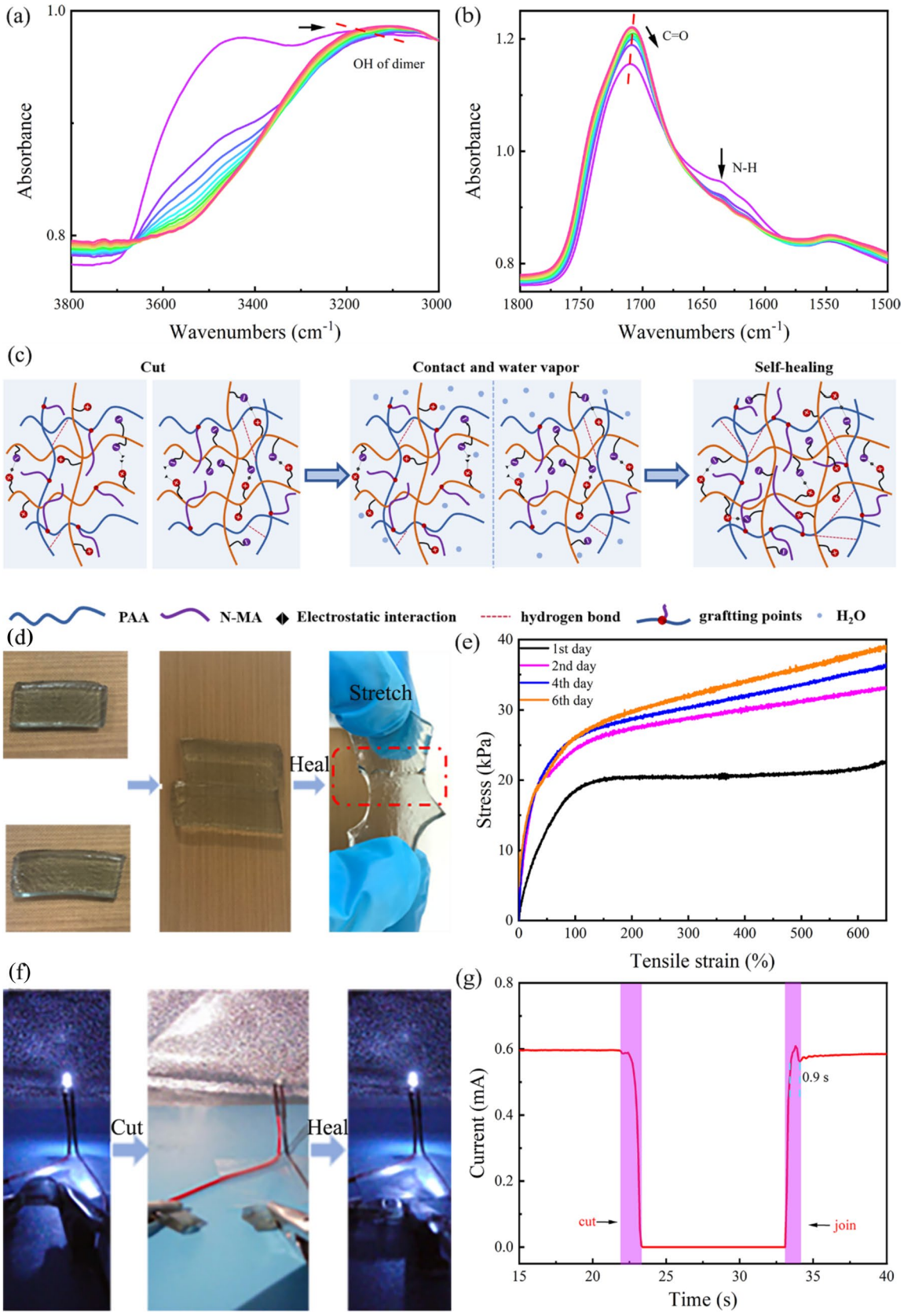
(a)
Absorbance
OH of dimer
Wavenumbers (cm-1)
(b)
C=O
N-H
Absorbance
Wavenumbers (cm-1)
(c)
Cut
Contact and water vapor
Self-healing
PAA
N-MA
Electrostatic interaction
hydrogen bond
graftting points
H2O
(d)
Heal
Stretch
(e)
1st day
2nd day
4th day
6th day
Stress (kPa)
Tensile strain (%)
(f)
Cut
Heal
(g)
Current (mA)
0.9 s
cut
join
Time (s)

◂**Fig. 4** Self-healing properties of P(AA-co–N-MA)/PEDOT: PSS hydrogel. Temperature-variable FTIR spectra of P(AA-co–N-MA)/PEDOT: PSS hydrogel is heating from 20 to 80 ℃ in the regions of **a** OH of the dimer and **b** ν(C = O), ν(N–H) (interval: 5 ℃). **c** Illustration of internal interaction and self-healing mechanism of P(AA-co–N-MA)/PEDOT: PSS hydrogel. **d** Pictures of the self-healing process of P(AA-co–N-MA)/PEDOT: PSS hydrogel. **e** Stretching curves of P(AA-co–N-MA)/PEDOT: PSS hydrogel after being stretched continuously for several self-healing cycles at 650% fixed. **f** The P(AA-co–N-MA)/PEDOT: PSS hydrogel acts as a conductor to connect the circuit and the LED bulb, which embodies the self-healing conductivity of the P(AA-co–N-MA)/PEDOT: PSS hydrogel. **g** The change of current in the P(AA-co–N-MA)/PEDOT: PSS hydrogel over time when it is complete, cut, and connected

the tensile strain of the hydrogel, indicating that the hydrogel has the potential as a sensor. The specific process and the illuminance change of the rebound process are shown in Figs. S9 and S10. The result is echoed by the relative resistance of P(AA-co–N-MA)/PEDOT:PSS hydrogel, as depicted in Fig. S11a. Evaluate strain sensitivity through gauge factor, $GF = (\Delta R/R_0)/\varepsilon$, and sensing range. To monitor various subtle or significant deformations, a sensor with high GF and a wide sensing range is required [50]. As a mechanically responsive flexible sensing material, the relative resistance of the hydrogel as a strain sensor increases exponentially, with the maximum tensile strain reaching 650%. The P(AA-co–N-MA)/PEDOT:PSS hydrogel strain sensor shows two linear regions according to different slopes. The GF of the sensor is 2.42 within 200% strain, and it grows to 8.14 when it exceeds 200%. These results show that P(AA-co–N-MA)/PEDOT:PSS hydrogel strain sensor showed high sensitivity to realize multi-directional monitoring and identification no matter what strain is. In addition, the resistance changes of different degrees of deformation are detected. Stretching P(AA-co–N-MA)/PEDOT:PSS hydrogel to fixed strains at 50%, 100%, 150%, and 200% produces repeatable strain-dependent resistance changes (Fig. S11b).

Furthermore, the ability of the hydrogel to act as a strain sensor is demonstrated by directly adhering to the material and bending to produce a reliable electrical response (Fig. S11c). In addition, when continuously bent at a fixed angle (0–90°), the resistance changes of the hydrogel showed excellent stability and repeatability (Fig. 5d), indicating its outstanding durability. The P(AA-co–N-MA)/PEDOT:PSS hydrogel–based flexible sensor has tremendous potential in detecting strain in time, which is essential in flexible electronics.

A soil moisture sensor is required to quickly measure the moisture content of the soil since soil moisture is often assessed by volumetric soil–water content [51]. Consequently, it was determined how the conductivity and water content of P(AA-co–N-MA)/PEDOT:PSS hydrogel changed over time and at various temperatures (Fig. 6 and Table S2). The water content of hydrogel gradually reduced as the temperature rose. The conductivity of hydrogel did not significantly diminish at 25 ℃ when the water content dropped. The conductivity of hydrogel did, however, visibly fall as the temperature increased along with the water content.

The strong correlation between environmental parameters and the conductivity of the P(AA-co–N-MA)/PEDOT:PSS hydrogel makes it a promising candidate for intelligent irrigation systems monitoring soil moisture levels. Agriculture, the predominant consumer of water, accounts for a substantial 62% of total water usage in economic and social sectors, with some regions witnessing an even higher share of 90%. The considerable potential for water conservation arises from the prevailing inefficiencies in water utilization within the agricultural sector. Agricultural irrigation increasingly shifts to more efficient and intelligent models confined to programmable or manual remote irrigation. Furthermore, the hydrogel demonstrates environmental friendliness, as substantiated by the Material Safety Data Sheet (MSDS), which indicates that the raw materials employed in hydrogel preparation, apart from N-MA, possess low toxicity and achieve near-toxicity-free status after polymerization [52].

Therefore, we have conceptualized an intelligent irrigation system utilizing P(AA-co–N-MA)/PEDOT:PSS hydrogel to enhance irrigation efficiency and conserve water resources essential for agricultural needs. The hydrogel is applied as a solenoid valve controller enables the creation of a flexible hydrogel sensor capable of autonomously regulating the irrigation valve switch by detecting changes in conductivity. On-demand control strategies for irrigation, rather than bypass control, optimize water utilization.

As depicted in Fig. 6, the irrigation process is triggered when the conductivity of hydrogel drops below a specific threshold (0.06 S/m), indicating insufficient water content within the hydrogel. Consequently, the valve opens automatically for irrigation. Conversely, if the conductivity remains above the threshold, it signifies sufficient soil moisture, leading to the exclusion of unnecessary irrigation. The flexibility of this sensor empowers on-demand irrigation based on soil moisture levels, effectively contributing to water conservation, which holds paramount importance given the global water supply situation. Moreover, the versatility of hydrogel in accommodating a wide range of temperatures makes it particularly suitable for various geographical contexts, particularly in deserts. As evident from Fig. 6, the conductivity of hydrogel diminishes over time as the water content exceeds 35 ℃. However, at 25 ℃, the conductivity demonstrates no significant trend, indicating the ability of the hydrogel to maintain stable conductivity at room temperature for a certain duration. In such an environment, soil moisture remains stable, obviating the need for irrigation. Furthermore, the conductivity and water content changes of hydrogel were monitored at room temperature under 10% relative humidity (Fig. S12). The water content of hydrogel

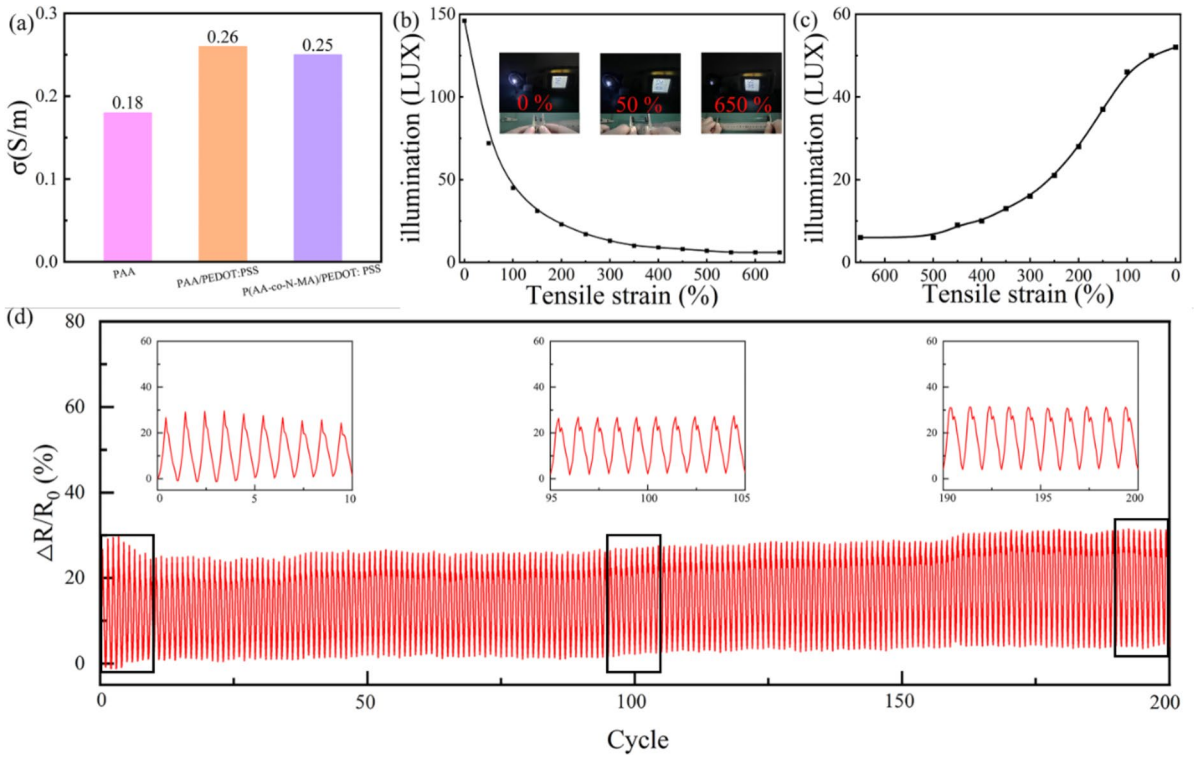

Fig. 5 Electrochemical and sensing properties of hydrogels. **a** Conductivity of PAA, PAA/PEDOT: PSS, and P(AA-co–N-MA)/PEDOT: PSS hydrogel. **b** The relationship between LED bulb illumination and the tensile strain of P(AA-co–N-MA)/PEDOT: PSS hydrogel. **c** The relationship between LED bulb illumination and the rebound process of P(AA-co–N-MA)/PEDOT: PSS hydrogel. **d** Relative resistance changes and the enlarged view of the marked area under more than 200 cycles of continuous bending at a fixed angle (0–90°)

exhibited a gradual decrease over 4 h, while the conductivity experienced a significant reduction after the same duration (Fig. S11a). By calculating the sensitivity of the hydrogel to water content, $GF = (\Delta R/R_0)$/water content, through the detection of resistance changes under varying water content conditions, the sensitivity value was determined to be 0.48 at

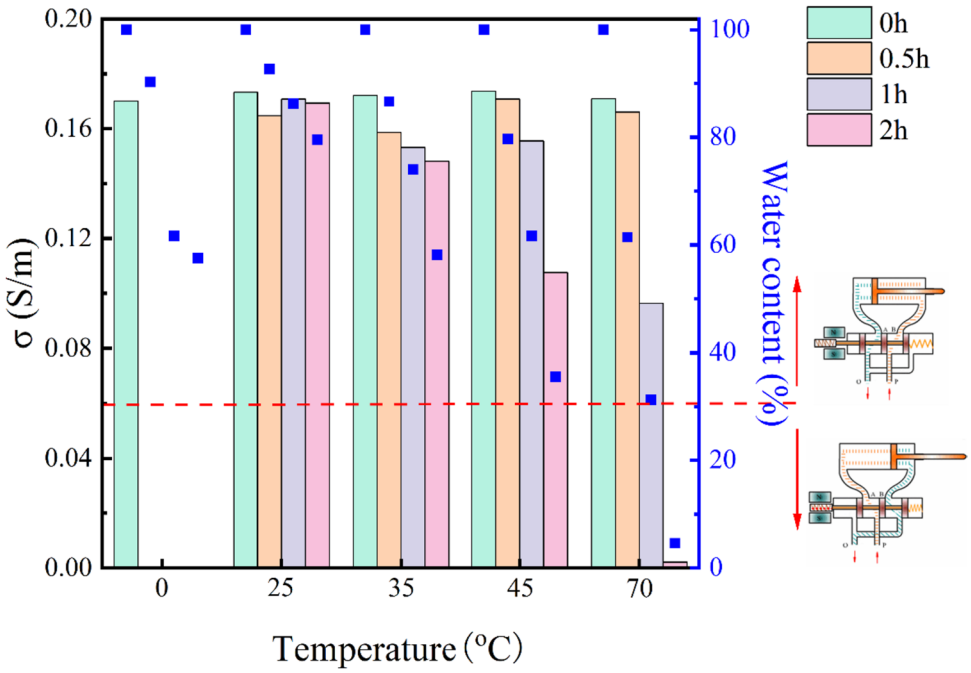

Fig. 6 Variations of conductivity and water content of the P(AA-co–N-MA)/PEDOT: PSS hydrogel over time at different temperatures and a schematic diagram for use as a solenoid valve controller (blue spots: water content; histogram: σ)

room temperature. These results demonstrate that the hydrogel maintains stable conductivity even in dry environments for a certain period, rendering it suitable for intelligent irrigation applications.

4 Conclusion

This study presents a green and gentle synthetic method for an intelligent material called P(AA-co–N-MA)/PEDOT:PSS hydrogel, enabling it to be used for mechanical sensing and soil moisture monitoring. Because of the complicated process and the development of industrialization, the synthesis of PAA-based hydrogels was improved. The reaction condition was lowered by using Na_2SO_3-APS as the initiator, allowing the reaction to be synthesized under relaxed circumstances for 10 min at 45 ℃. The crosslinked network P(AA-co–N-MA) was given the PEDOT:PSS network, and the dual network structure resulted in a mechanically sensitive flexible sensing material. Even at high temperatures, P(AA-co–N-MA)/PEDOT:PSS hydrogel demonstrates good mechanical characteristics. It possesses remarkable elasticity and fatigue resistance, and the elongation at break reached 2400% at RT. Compared to several flexible sensing materials, P(AA-co–N-MA)/PEDOT:PSS hydrogel has a higher GF of up to 8.14 at the same strain (such as hydrogels, organic gels, ionic gels, conductive elastomers). P(AA-co–N-MA)/PEDOT:PSS hydrogel has susceptible mechanical sensing properties, which was explained by the strain-dependent resistance change of the hydrogel. Furthermore, P(AA-co–N-MA)/PEDOT:PSS hydrogel has the capacity for self-healing, particularly in humid settings. Additionally, the variations in the water content and conductivity of hydrogel throughout a broad range of valuable temperatures offer fresh concepts for on-demand irrigation of intelligent irrigation systems, which would be crucial for water conservation.

Supplementary Information The online version contains supplementary material available at https://doi.org/10.1007/s42114-023-00821-2.

Author contribution Fang-Chang Tsai and Ning Ma conceived the research, designed the experiments, and co-wrote the paper. Xue-Qing Zhan co-wrote the paper, too. Xue-Qing Zhan and Zhuo-Qing Ran prepared the materials and conducted thermodynamic tests. Xue-Qing Zhan, Hong-Yu Bao, Zhuo-Qing Ran, Han Chen, Qiang Fu, Wang Ni, and Jia-Ming Xu performed the mechanical and optical performance testing. Xue-Qing Zhan, Qin Ye, Fang-Chang Tsai, and Ning Ma performed the reaction mechanism. Xue-Qing Zhan carried out and analyzed all experimental data. All the authors discussed the results and contributed to writing the manuscript. All authors reviewed the manuscript.

Funding This study was funded by the National Natural Science Foundation of China (52203161), Key Research and Development Plan of Hubei Province (2022BAD029), Technical Innovation and Development Project of Hubei Province (High-tech Enterprises) (2021BAB085), and Supported by Open Funding Project of the State Key Laboratory of Biocatalysis and Enzyme Engineering (SKLBEE2021031).

Data availability Data available within the article or its supplementary materials.

Code availability The code used to develop individual figures is available upon request to the corresponding author.

Declarations

Competing interests The authors declare no competing interests.

References

1. Koehler A (2008) Water use in LCA: managing the planet's freshwater resources. Int J Life Cycle Ass 13:451–455. https://doi.org/10.1007/s11367-008-0028-6
2. Ding C, Zhang S, Fu X, Liu T, Shao L, Fei M, Hao C, Liu Y, Zhong WH (2021) Robust supramolecular composite hydrogels for sustainable and "visible" agriculture irrigation. J Mater Chem A 9:24613–24621. https://doi.org/10.1039/d1ta05442b
3. Oladosu Y, Rafii MY, Arolu F, Chukwu SC, Salisu MA, Fagbohun IK, Muftaudeen TK, Swaray S, Haliru BS (2022) Superabsorbent polymer hydrogels for sustainable agriculture: a review. Horticulturae 8:e8070605. https://doi.org/10.3390/horticulturae8070605
4. Palanivelu SD, Armir NAZ, Zulkifli A, Hair AHA, Salleh KM, Lindsey K, Che-Othman MH, Zakaria S (2022) Hydrogel application in urban farming: potentials and limitations-a review. Polymers-Basel 14:2590. https://doi.org/10.3390/polym14132590
5. Dhiman J, Prasher SO, ElSayed E, Patel RM, Nzediegwu C, Mawof A (2021) Effect of hydrogel based soil amendments on heavy metal uptake by spinach grown with wastewater irrigation. J Clean Prod 311:127644. https://doi.org/10.1016/j.jclepro.2021.127644
6. Yu F, Yang P, Yang Z, Zhang X, Ma J (2021) Double-network hydrogel adsorbents for environmental applications. Chem Eng J 426:131900. https://doi.org/10.1016/j.cej.2021.131900
7. Mu R, Liu B, Chen X, Wang N, Yang J (2020) Hydrogel adsorbent in industrial wastewater treatment and ecological environment protection. Environ Technol Inno 20:101107. https://doi.org/10.1016/j.eti.2020.101107
8. Zhan XQ, Yu XY, Tsai FC, Ma N, Liu HL, Han Y, Xie L, Jiang T, Shi D, Xiong Y (2018) Magnetic MOF for AO7 removal and targeted delivery. Crystals 8:250. https://doi.org/10.3390/cryst8060250
9. Zhan XQ, Tsai FC, Xie L, Zhang KD, Liu HL, Ma N, Shi D, Jiang T (2018) Ligands-coordinated Zr-based MOF for wastewater treatment. Nanomaterals-Basel 8:655–668. https://doi.org/10.3390/nano8090655
10. Zhang KD, Tsai FC, Ma N, Xia Y, Liu HL, Zhan XQ, Yu XY, Zeng XZ, Jiang T, Shi D, Chang CJ (2017) Adsorption behavior of high stable Zr-based MOFs for the removal of acid organic dye from water. Materals-Basel 10:205. https://doi.org/10.3390/ma10020205
11. Zhan XQ, Zhang Y, Xie L, Liu HL, Zhang XK, Ruan B, Ding H, Wu J, Shi D, Jiang T, Ma N, Tsai F-C (2020) Magnetically treated Zr-based UiO-type porous coordination polymers study on adsorption of azo dye. Micropor Mesopor Mat 306:110291. https://doi.org/10.1016/j.micromeso.2020.110291
12. Wang C, Liu X, Yang T, Sridhar D, Algadi H, Bin XuB, El-Bahy ZM, Li H, Ma Y, Li T, Guo Z (2023) An overview of metal-organic frameworks and their magnetic composites for the removal of pollutants. Sep Purif Technol 320:124144. https://doi.org/10.1016/j.seppur.2023.124144

13. Kang F, Jiang X, Wang Y, Ren J, Xu BB, Gao G, Huang Z, Guo Z (2023) Electron-rich biochar enhanced Z-scheme heterojunctioned bismuth tungstate/bismuth oxyiodide removing tetracycline. Inorg Chem Front. https://doi.org/10.1039/d3qi01283b
14. Zeng J, Xie W, Guo Y, Zhao T, Zhou H, Wang Q, Li H, Guo Z, Xu BB, Gu H (2024) Magnetic field facilitated electrocatalytic degradation of tetracycline in wastewater by magnetic porous carbonized phthalonitrile resin. Appl Catal B-Environ 340:123225. https://doi.org/10.1016/j.apcatb.2023.123225
15. Zhang F, Lian M, Alhadhrami A, Huang M, Li B, Mersal GAM, Ibrahim MM, Xu M (2022) Laccase immobilized on functionalized cellulose nanofiber/alginate composite hydrogel for efficient bisphenol A degradation from polluted water. Adv Compos Hybrid Mater 5:1852–1864. https://doi.org/10.1007/s42114-022-00476-5
16. Chang X, Li S, Li N, Wang S, Li J, Guo C, Yu L, Murto P, Xu X (2022) Marine biomass-derived, hygroscopic and temperature-responsive hydrogel beads for atmospheric water harvesting and solar-powered irrigation. J Mater Chem A 10:18170–18184. https://doi.org/10.1039/d2ta04919h
17. Zhou X, Guo Y, Zhao F, Shi W, Yu G (2020) Topology-controlled hydration of polymer network in hydrogels for solar-driven wastewater treatment. Adv Mater 32:e2007012. https://doi.org/10.1002/adma.202007012
18. Zhang Z, Fu H, Li Z, Huang J, Xu Z, Lai Y, Qian X, Zhang S (2022) Hydrogel materials for sustainable water resources harvesting & treatment: synthesis, mechanism and applications. Chem Eng J 439:135756. https://doi.org/10.1016/j.cej.2022.135756
19. Yang S, Shi C, Qu K, Sun Z, Li H, Xu B, Huang Z, Guo Z (2023) Electrostatic self-assembly cellulose nanofibers/MXene/nickel chains for highly stable and efficient seawater evaporation and purification. Carbon Lett. https://doi.org/10.1007/s42823-023-00540-0
20. Vera J, Conejero W, Mira-García AB, Conesa MR, Ruiz-Sánchez MC (2021) Towards irrigation automation based on dielectric soil sensors. J Hortic Sci Biotechnol 96:696–707. https://doi.org/10.1080/14620316.2021.1906761
21. Kabir MH, Ahmed K, Furukawa H (2017) A low cost sensor based agriculture monitoring system using polymeric hydrogel. J Electrochem Soc 164:B3107–B3112. https://doi.org/10.1149/2.0171705jes
22. Romero MR, Trejo Nieva G, Vedelago J, Gomez CG (2021) A microfluidic actuator based on a stimuli-responsive hydrogel grafted into Cucurbita moschata xylems. Soft Matter 17:5941–5949. https://doi.org/10.1039/d1sm00162k
23. Romero R, Muriel JL, García I, Muñoz de la Peña D (2012) Research on automatic irrigation control: State of the art and recent results. Agr Water Manage 114:59–66. https://doi.org/10.1016/j.agwat.2012.06.026
24. Medici LO, Rocha HSd, Carvalho DFd, Pimentel C, Azevedo RA (2010) Automatic controller to water plants. Sci Agr 67:727–730. https://doi.org/10.1590/S0103-90162010000600016
25. Surya SG, Yuvaraja S, Varrla E, Palaparthy BMS, VS, Salama KN, (2020) An in-field integrated capacitive sensor for rapid detection and quantification of soil moisture. Sensor Actuat B-Chem 321:128542. https://doi.org/10.1016/j.snb.2020.128542
26. Santos HTd, Carvalho DFd, Souza CF, Medici LO (2015) Cultivo de alface em solos com hidrogel utilizando irrigação automatizada. Engenharia Agrícola 35:852–862. https://doi.org/10.1590/1809-4430-Eng.Agric.v35n5p852-862/2015
27. Hardie M (2020) Review of novel and emerging proximal soil moisture sensors for use in agriculture. Sensors-Basel 20:6934. https://doi.org/10.3390/s20236934
28. Wang T, Yi W, Zhang Y, Wu H, Fan H, Zhao J, Wang S (2023) Sodium alginate hydrogel containing platelet-rich plasma for wound healing. Colloids Surf B Biointerfaces 222:113096–113104. https://doi.org/10.1016/j.colsurfb.2022.113096
29. Ouyang Y, Zhao J, Wang S (2023) Multifunctional hydrogels based on chitosan, hyaluronic acid and other biological macromolecules for the treatment of inflammatory bowel disease: a review. Int J Biol Macromol 227:505–523. https://doi.org/10.1016/j.ijbiomac.2022.12.032
30. Chen Z, Yao J, Zhao J, Wang S (2023) Injectable wound dressing based on carboxymethyl chitosan triple-network hydrogel for effective wound antibacterial and hemostasis. Int J Biol Macromol 225:1235–1245. https://doi.org/10.1016/j.ijbiomac.2022.11.184
31. Hua J, Björling M, Larsson R, Shi Y (2021) Friction control of chitosan-Ag hydrogel by silver ion. ES Mater Manuf 16:30–36. https://doi.org/10.30919/esmm5f555
32. Montesano FF, Parente A, Santamaria P, Sannino A, Serio F (2015) Biodegradable superabsorbent hydrogel increaseswater retention properties of growing media and plant growth. Agric AgricSci Procedia 4:451–458. https://doi.org/10.1016/j.aaspro.2015.03.052
33. Chaudhary J, Thakur S, Sharma M, Gupta VK, Thakur VK (2020) Development of biodegradable agar-agar/gelatin-based superabsorbent hydrogel as an efficient moisture-retaining agent. Biomolecules 10:939. https://doi.org/10.3390/biom10060939
34. Hafsa B, Reddy SG, Kumar BS, Prashanthi K, Murthy HC (2023) Modified layered double hydroxide–PEG magneto-sensitive hydrogels with suitable ligno-alginate green polymer composite for prolonged drug delivery applications. Eng Sci 24:914. https://doi.org/10.30919/es914
35. Li T, Wei H, Zhang Y, Wan T, Cui D, Zhao S, Zhang T, Ji Y, Algadi H, Guo Z, Chu L, Cheng B (2023) Sodium alginate reinforced polyacrylamide/xanthan gum double network ionic hydrogels for stress sensing and self-powered wearable device applications. Carbohyd Polym 309:120678. https://doi.org/10.1016/j.carbpol.2023.120678
36. Wu Y, Liu J, Lin S, Huang K, Chen E, Huang K, Lei M (2022) A new pressure matrix array sensor composed of flexible mechanical sensor elements. Eng Sci 18:105–112. https://doi.org/10.30919/es8d626
37. Liu J, Chen E, Wu Y, Yang H, Huang K, Chang G, Pan X, Huang K, He Z, Lei M (2022) Silver nanosheets doped polyvinyl alcohol hydrogel piezoresistive bifunctional sensor with a wide range and high resolution for human motion detection. Adv Compos Hybrid Mater 5:1196–1205. https://doi.org/10.1007/s42114-022-00472-9
38. Wu Y, Chen E, Weng X, He Z, Chang G, Pan X, Liu J, Huang K, Huang K, Lei M (2022) Conductive polyvinyl alcohol/silver nanoparticles hydrogel sensor with large draw ratio, high sensitivity and high stability for human behavior monitoring. Eng Sci. https://doi.org/10.30919/es8d659
39. Shen Y, Yang W, Hu F, Zheng X, Zheng Y, Liu H, Algadi H, Chen K (2022) Ultrasensitive wearable strain sensor for promising application in cardiac rehabilitation. Adv Compos Hybrid Mater 6:21. https://doi.org/10.1007/s42114-022-00610-3
40. Huang K, Wu Y, Liu J, Chang G, Pan X, Weng X, Wang Y, Lei M (2022) A double-layer CNTs/PVA hydrogel with high stretchability and compressibility for human motion detection. Eng Sci 17:319–327. https://doi.org/10.30919/es8d625
41. Kong D, El-Bahy ZM, Algadi H, Li T, El-Bahy SM, Nassan MA, Li J, Faheim AA, Li A, Xu C, Huang M, Cui D, Wei H (2022) Highly sensitive strain sensors with wide operation range from strong MXene-composited polyvinyl alcohol/sodium carboxymethylcellulose double network hydrogel. Adv Compos Hybrid Mater 5:1976–1987. https://doi.org/10.1007/s42114-022-00531-1
42. Shao C, Meng L, Cui C, Yang J (2019) An integrated self-healable and robust conductive hydrogel for dynamically self-adhesive and highly conformable electronic skin. J Mater Chem C 7:15208–15218. https://doi.org/10.1039/c9tc05467g
43. Shi X, Wu P (2021) A smart patch with on-demand detachable adhesion for bioelectronics. Small 17:e2101220. https://doi.org/10.1002/smll.202101220

44. Wang M, Lai Z, Jin X, Sun T, Liu H, Qi H (2021) Multifunctional liquid-free ionic conductive elastomer fabricated by liquid metal induced polymerization. Adv Func Mater 31:2101957. https://doi.org/10.1002/adfm.202101957
45. Zhang W, Wu B, Sun S, Wu P (2021) Skin-like mechanoresponsive self-healing ionic elastomer from supramolecular zwitterionic network. Nat Commun 12:4082. https://doi.org/10.1038/s41467-021-24382-4
46. Bai W, Zhang L, Bai R, Zhang G (2008) A very useful redox initiator for aqueous RAFT polymerization of N-Isopropylacrylamide and acrylamide at room temperature. Macromol Rapid Comm 29:562–566. https://doi.org/10.1002/marc.200700823
47. Junsoo K, Zhang G-G, Shi MX, Suo Z (2021) Fracture, fatigue, and friction of polymers in which entanglements greatly outnumber crosslinks. Science 374:212–216
48. Zhang M, Wang R, Shi Z, Huang X, Zhao W, Zhao C (2017) Multi-responsive, tough and reversible hydrogels with tunable swelling property. J Hazard Mater 322:499–507. https://doi.org/10.1016/j.jhazmat.2016.10.016
49. Zhou Q, Lyu J, Wang G, Robertson M, Qiang Z, Sun B, Ye C, Zhu M (2021) Mechanically strong and multifunctional hybrid hydrogels with ultrahigh electrical conductivity. Adv Func Mater 31:2104536. https://doi.org/10.1002/adfm.202104536
50. Liang L, Lv H, Shi XL, Liu Z, Chen G, Chen ZG, Sun G (2021) A flexible quasi-solid-state thermoelectrochemical cell with high stretchability as an energy-autonomous strain sensor. Mater Horiz 8:2750–2760. https://doi.org/10.1039/d1mh00775k
51. Topp GC, Ferré TPA (2002) Methods of soil analysis: part 4 physical methods. Soil Sci Soc Am 417–545
52. Erkekoglu P, Baydar T (2014) Acrylamide neurotoxicity. Nutr Neurosci 17:49–57. https://doi.org/10.1179/1476830513Y.0000000065